2024 IEEE International Conference on Robotics and Automation (ICRA 2024)
May 13-17, 2024. Yokohama, Japan

Automated Assembly by Two-Fingered Microhand for Fabrication of Soft Magnetic Microrobots

Yue Zhao, Xiaoming Liu, *Member*, *IEEE*, Ruixi Wang, Dan Liu, Masaru Kojima, Qiang Huang, *Fellow*, *IEEE*, and Tatsuo Arai, *Life Fellow*, *IEEE*

***Abstract*— Micro-assembly is an emerging method to fabricate microrobots with multiple modules or particles. However, there is always a lack of a flexible and efficient method to freely create the desired magnetic soft microrobots. In this paper, an automated assembly system based on a two-fingered microhand is presented for fabricating magnetic soft microrobots. Our proposed system can automatically pick and place components to assemble microrobots with a two-fingered micromanipulator, and orient these components through an external magnetic field. The automated assembly has the advantages of high accuracy, high speed, and high success rate. It can endow magnetic microrobots with flexible material selection, arbitrary geometry design, and programable magnetization profile. We can make full use of this system to fabricate multiple magnetic soft microrobots. The experiment results demonstrate that this system can efficiently fabricate microrobots with excellent mechanical properties, which have application potential in robotics, biomedical engineering, and environmental governance.**

I. Introduction

Microrobots, due to their unique feature of minute size [1]-[3], have shown many promising applications in early diagnosis, microsurgery, targeted drug delivery, and disease monitoring [4]-[7]. The magnetic field is the ideal energy source to actuate microrobots compared to other strategies [8]-[12], as it enables wireless actuation, fast response, high precision, and stable control [13]-[15]. In the past two decades, various magnetic microrobot fabrication methods including stereolithographic 3D printing, extrusion printing, heating, mold casting, laser cutting, and chemical self-assembly or synthesis have been proposed. However, more advanced capabilities based on arbitrary geometry design, flexible material selection, and programable magnetization patterns are required for the clinical applications of magnetic microrobots, posing significant challenges in the fabrication process.

Micro-assembly is the process of creating micromachines with multiple components using controllable high-precision micromanipulation technology. It can fabricate the magnetic microrobots by assembling the pre-magnetized micro modules or particles with precise control of position and orientation. This assembly-based fabrication method enables the integration of multiple materials and the formation of sufficient local magnetic torque vectors in desired orientations. Larger design space of the magnetic microrobots is achieved and the machine functionality is substantially enhanced. Micro-assembly can greatly extend possibilities toward microrobots with reprogrammable magnetization, shape reconfiguration, and multiple functions. It can create powerful microrobots tailored to specific biomedical applications, with sizes ranging from microns to millimeters.

Traditional tool-assisted manual assembly is still widely used for fabricating module-based microrobots. Zhang et al. fabricated an untethered 12-legged microrobot by assembling magnetic-responsive elastomers and liquid crystal elastomers via the connection pads with the assistance of the negative molds [16]. Dong et al. constructed an untethered magnetic soft microrobot by embedding the programmed magnetization modules and the spatially distributed functional modules into the adhesive sticker layers [17]. With the miniaturization of assembly modules, Zhang et al. proposed a jig-assisted 3D bottom-up assembly strategy, which can assemble multi-material heterogeneous microscale building blocks called “voxels” [18]. However, the resolution of these fabricated microrobots is restricted by the precision of human operation, and the fabrication process is labor-intensive. 3D printing, as its high resolution and full programmability, has been employed for microrobot assembly [19]-[22]. The comparison of resolution can be found in TABLE I. However, the complex and cumbersome fabrication process and the difficulties in integrating multiple materials and functional modules hinder its wide application.

TABLE I. Resolution Comparison of previous techniques

Techniques	Resolution	Ref
Mold casting/jig-assisted manual assembly	0.1~1mm	[16]-[18]
3D printing & UV lithography	100~250μm	[19], [20]
Molding-integrated direct laser writing	10~100μm	[21]
Two-photon polymerization	1~10μm	[22]

Here, we report an automated assembly system for magnetic soft microrobot fabrication. As shown in Figure 1,

This work was supported by the National Natural Science Foundation of China under Grant 62273052, the Beijing Natural Science Foundation under Grant IS23062, China Postdoctoral Science Foundation under Grant 2022M710378 and the Grant-in-Aid for Scientific Research under Grant 22H01441 from the Ministry of Education, Culture, Sports, Science and Technology of Japan. *(Corresponding author: Xiaoming Liu.)*

Y. Zhao, X. Liu, R. Wang, D. Liu, Q. Huang, and T. Arai are with the Key Laboratory of Biomimetic Robots and Systems, Ministry of Education, State Key Laboratory of Intelligent Control and Decision of Complex System, Beijing Advanced Innovation Center for Intelligent Robots and Systems, and School of Mechatronical Engineering, Beijing Institute of Technology, Beijing 100081, China (e-mail: liuxiaoming555@ bit.edu.cn).

R. Wang is also with the Department of Intelligent Manufacturing, Shenzhen International Graduate School of Tsinghua University, Shenzhen 518057, China. M. Kojima is with the Department of Materials Engineering Science, Osaka University, Toyonaka, Osaka 560-8531, Japan. T. Arai is also with Center for Neuroscience and Biomedical Engineering, The University of Electro-Communications, Tokyo 1828585, Japan.

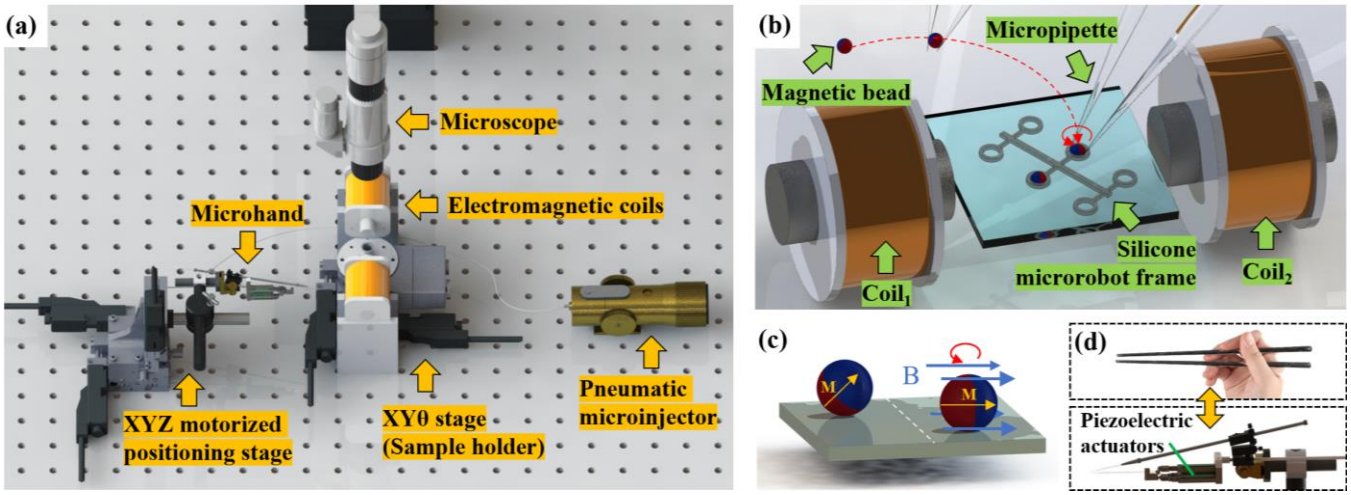

Figure 1. (a) Overview of the proposed assembly system. (b) Schematic diagram of micro-assembly method by two-fingered microhand under magnetic field. (c) Moving schematic of the rotation of magnetic microbead in constant magnetic flux density. (d) Two-fingered microhand modeled after chopsticks.

this assembly system uses a two-fingered microhand to place magnetic microbeads on the laser-cut soft frame. The external magnetic field is employed for the orientation of microbeads, which enables the customizable magnetization profiles. Compared to previous methods, this system has the advantages of enormous manipulation freedom, high operation accuracy, and automatable capability. It has been proved that this micro-assembly method can fabricate diverse magnetic soft microrobots automatically in a relatively short time. The experiment results show that the assembled microrobots have excellent mechanical properties and different locomotion modes for expected applications in robotics, biomedical engineering, and environmental governance.

II. System Setup

As shown in Figure 2, the micro-assembly system mainly included three sub-systems: the motion system, the magnetic control system, and the vision system. The motion system was utilized to position the soft frame (microrobot body) and magnetic microbeads (magnetically actuated components), as well as orient the frame by rotation actuator. Then, the magnetic control system was responsible for orientating the released magnetic microbeads inside the holes of the frame. The vision system could send real-time image information to provide visual feedback for automated assembly. All sub-systems were controlled through a PC (Windows).

The motion system was mainly conducted by a piezo-driven two-fingered microhand mounted on a 3-DoF motorized positioning stage, and a 2-DoF stage with a rotation actuator. Similar to chopsticks as shown in Figure 1(d), the two-fingered microhand was used to grasp the pre-magnetized microbeads and release them at the desired position. One of the two fingers was driven by piezoelectric ceramics to adjust the distance between two needle tips for grasping and releasing the target, while the other finger was connected to a pneumatic microinjector to dispense UV curing adhesives for bonding different components. The whole microhand was held by the X-Y-Z stage and could be moved in a large 3-D workspace, which enabled the assembly of magnetic soft robots from microscale to macroscale. The X-Y-θ stage (sample holder) was utilized to position the microrobot soft frame and rotate it to form a proper angle difference with the magnetic field direction for the next step of the released microbead orientation.

The microhand was a 3-DoF parallel mechanism driven by three piezoelectric actuators [23], [24]. The motion of every joint was realized through the designed flexure hinge. The piezoelectric actuator (NEC TOKIN, AE0203D16), with a maximum extension of 17 μm, was driven by a voltage amplifier (Matsusada Precision Inc., PZJ-0.15P). Two strain gauges were orthogonally attached to the piezoelectric actuator for the close-loop control and hysteresis avoidance. The feedback signal was conditioned by the strain gauge bridge box and amplified by the amplifier (KYOWA, MCD-8A). The signal was then input into the microhand controller (AD chip ADC78H90, DA chip DAC-AD5363, MCU STM32 F767ZI) for AD conversion. The onboard motion control algorithm of both the microhand and stages was executed on this controller. The X-Y-Z stage (OptoSigma, TAM 655) was motorized by three linear motors (OptoSigma, SGSP-13ACT-B0) with a maximum travel distance of 13 mm and a maximum speed of 2 mm/s. The rotation actuator (OptoSigma, SGSP-60YAW-OB) was mounted on the X-Y stage with the same configuration as the X-Y-Z stage.

The magnetic control system was conducted by a pair of electromagnetic coils with 15000 turns. The control signal was first generated by a customized program in the PC and then transmitted through a serial port to the DA converter (DAC-AD5363). The power amplifier (Aigtek ATA-2022H China) was used to amplify the signal, which was output for the coils to generate desired magnetic fields. The coil bases and the base for holding the sample were both printed by a 3-D printer (Stratasys, uPrint SE). The exposure light source was UV LED (Zolix, M405L), with a minimum output power of 400mW and a wavelength of 405nm. All the experimental processes were recorded using a CCD camera (HIKROBOT, MV-CA050-11UM) that offered a framerate of up to 35 fps under a maximum resolution of 2448 × 2048. The real-time images were processed by computer vision (OpenCV 3.0), providing position and posture feedback to the microhand controller.

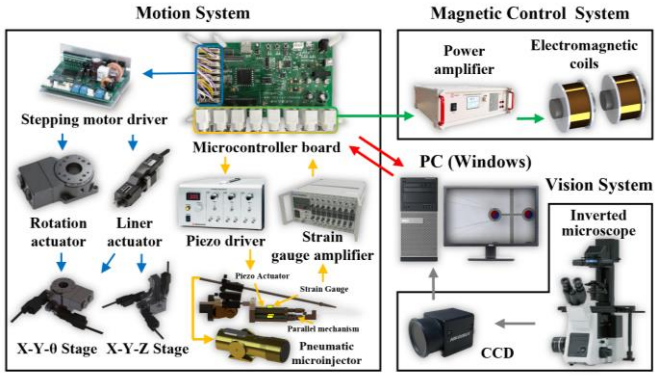

Figure 2. Configuration of the experimental system.

III. METHODS

A. Rotation of Magnetic Microbeads

As schematically illustrated in Figure 1(b) and Figure 1(c), magnetic microbeads can rotate under the actuation of a magnetic field with constant magnetic flux density. By applying a magnetic field with constant and uniform magnetic strength in space, a torque can drive the rotation of magnetic microbeads. This torque tends to rotate and align the microbead moment with the direction of the external field, which is denoted as

$$\vec{\tau} = \vec{M} \times B \tag{1}$$

where M is the net magnetic moment of the magnetic microbead, and B is the magnetic flux density.

B. Inverse Kinematics Analysis of 3D Parallel Mechanism

The schematic diagram of the joint structure in the 3-PRR (3-prismatic-revolute-revolute) mechanism is shown in Figure 3(a), and the inverse kinematics analysis is performed using geometric methods based on it. Establish a coordinate system O at the end-effector in Figure 3(a). The three degrees of freedom of the mechanism are linear translation along the X-axis due to P1, P2, and P3 deformations, rotational movement around the Z-axis due to P1 deformation, and rotational movement around the Y-axis due to P2 or P3 deformations. The parallel mechanism is divided into kinematic chain 1 and kinematic chain 2/3, and new coordinate systems are established for analysis separately, as shown in Figure 3(b) and Figure 3(c). The detailed calculation process is omitted here. Through geometric analysis, the relationship between the displacement of the end-effector and the displacement of each joint can be obtained, which is denoted as

$$\Delta p_1 = l_1 \cos\theta_1 + l_2 \sin\alpha - \sqrt{l_1^2 - x_a^2} \tag{2}$$

$$\Delta p_2 = l_4 \cos\theta_4 + l_5 \sin(\beta - \theta_3) - \sqrt{l_4^2 - B'H^2} \tag{3}$$

$$\Delta p_3 = -\Delta p_2 \tag{4}$$

where Δp is the displacement of each prismatic joint, and the definitions of l, θ, α, β, etc. are marked in Figure 3. The inverse kinematic solution of the 3D parallel mechanism can be obtained by combining (2), (3) and (4):

$$p = [p_1, p_2, p_3]^T = [\Delta p_1 + x, \Delta p_2 + x, \Delta p_3 + x]^T \tag{5}$$

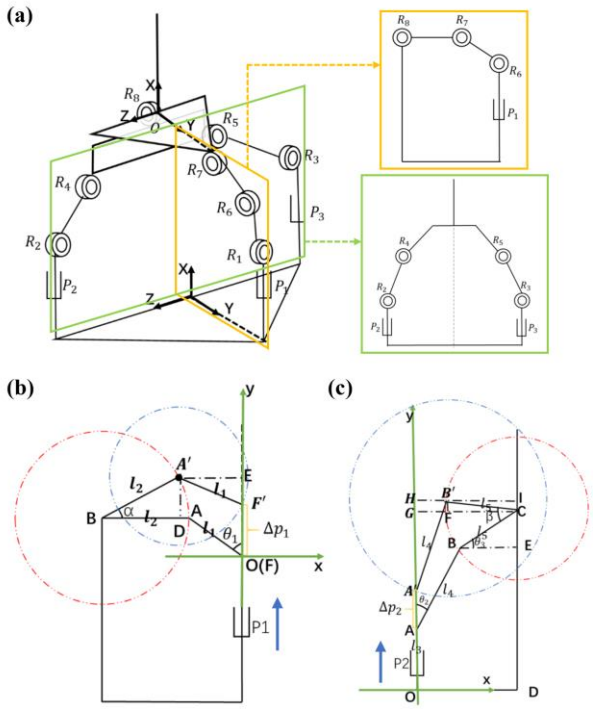

Figure 3. (a) Schematic diagram of the joint structure of the 3D parallel mechanism. (b) Kinematic chain 1. (c) Kinematic chain 2/3.

where x is the displacement of each joint when three joints move together to achieve translational motion along the X-axis.

C. Automated Assembly Process

The automated assembly process has been achieved by the control of the microhand and the feedback of the computer vision. For example, Figure 4(a) shows the assembly process of a hexapod magnetic soft microrobot. Firstly, a single-axis uniform magnetic field was applied to the workspace through the electromagnetic coils. The microinjector-connected finger extracted UV-curing adhesives, and then grasped the magnetic microbead recognized through Hoff circle detection. The rotation actuator then rotated the sample holder 45 ° to the left, forming an angle difference between the magnetic field direction and the main axis of the soft frame. Next, the hole position of the soft frame was detected and the microhand holding microbead was moved above the target hole. After that, the pneumatic microinjector applied positive pressure to extrude a portion of UV-curing adhesives from the finger, dripping into the hole. Then, the microbead was quickly released and dropped into the hole filled with adhesives. Before the adhesives were fully cured, the magnetic field could drive the microbead to rotate until its direction aligned with the magnetic field direction. After a few seconds, the UV light source was turned on to expose the connection between the microbead and the soft frame for half a minute. In this way, the microbead was fixed in the soft frame according to our designed direction. For the hexapod magnetic soft microrobot, the microbead directions at four corners were consistent, so they could be assembled by repeating the same steps. For the two magnetic microbeads in the middle position, the frame needed to be rotated 90° to the right, and then the above steps were repeated to complete the assembly of the remaining magnetic microbeads in different directions.

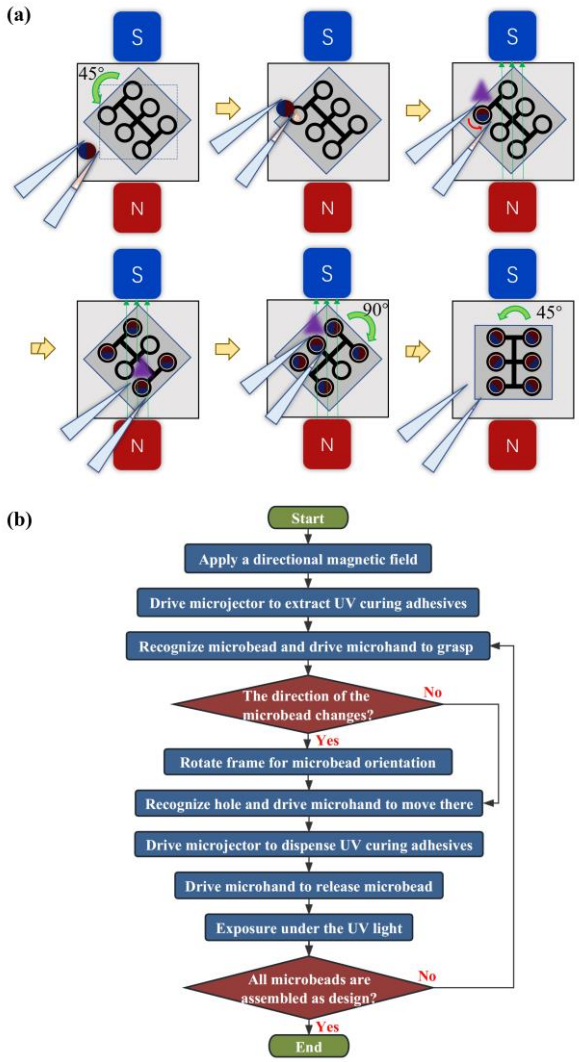

Figure 4. (a) The assembly process of a hexapod magnetic soft microrobot. (b) Flowchart of automated assembly for magnetic soft robot fabrication.

Figure 4(b) shows the flowchart of automated assembly, which can be applied to all magnetic soft robot fabrication by our method. For the hexapod microrobot with a body length of about 6mm, the average assembly time is 7.4 minutes and the success rate can reach approximately 85%. Failures usually occur due to the adhesion force of microbeads at the end-effector, which is addressed in the automated assembly process by detecting this situation through visual recognition and driving the end-effector to undergo high-frequency vibrations to shake off the microbead. The assembly time for other microrobots is approximately similar to that of the hexapod robot, mainly depending on the number of microbeads to be assembled. On the one hand, compared to traditional manual assembly using tweezers, this automated assembly method saves more time and avoids intensive labor. Moreover, the proposed assembly system has the potential to fabricate robots of tens of micrometers, thanks to the micrometer-level manipulation accuracy of the piezo-driven microhand. On the other hand, due to the use of a 3-DoF manipulator for operation in open space, our method has higher flexibility than assembly combined with 3D printing. The assembly materials, the operation steps, and the

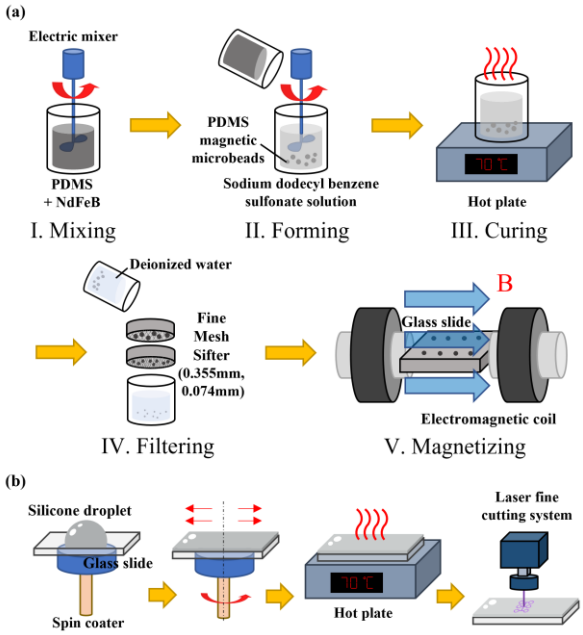

Figure 5. (a) The fabrication process of the PDMS magnetic microbeads. (b) The fabrication process of silicone soft frame by laser cutting.

microhand manipulation precision can be adjusted during assembly, which greatly improves fabrication efficiency.

IV. Results

A. Experimental Setup

A micropipette was selected as the end-effector of the microhand in our experiment, which was a hollow capillary glass tube (JITIAN BIO, BJ-40) with an outer diameter of 1mm, an inner diameter of 0.8mm, and a length of 100mm. Installed it on the needle puller (PC-100, Narishige Corporation, Japan) and pulled it into a needle tip shape. Then a needle grinder (EG-401, Narishige Corporation, Japan) was used to polish the needle tip to a size suitable for grasping.

The fabrication process of PDMS magnetic microbeads can be divided into six steps, as shown in Figure 5(a). Step 1: Mixing. Weighed PDMS solution and NdFeB powder of the same quality (1:1) with an electronic scale. Besides, the PDMS cross-linker (PDMS: cross-linker = 10:1) and silicone oil (PDMS: silicone oil = 5:1) were added into a glass beaker. Subsequently, the mixture was stirred to get a uniform distribution of NdFeB particles within the PDMS matrix using an electric mixer (JJ-1A blender with digital display). The stirring process was carried out at the speed of 600 rpm and lasted for 6 hours. The mixing effect was continuously observed during the stirring process by sampling. Step 2: Formation of beads. The mixture was degassed at room temperature and placed in a vacuum chamber for 20 minutes to remove the bubbles in the solution. The mixture was poured into 2 wt% sodium dodecylbenzene sulfonate solution. The spherical shape resulted from the inherent hydrophobic nature of PDMS. A stirring was used to form PDMS magnetic beads while pouring. Step 3: Curing. The obtained PDMS magnetic beads were cured at 70°C for 6 hours to form the PDMS magnetic micro-balls. Step 4: Cleaning and collection. The cured PDMS magnetic beads were cleaned with deionized water. The solution containing the beads was poured and

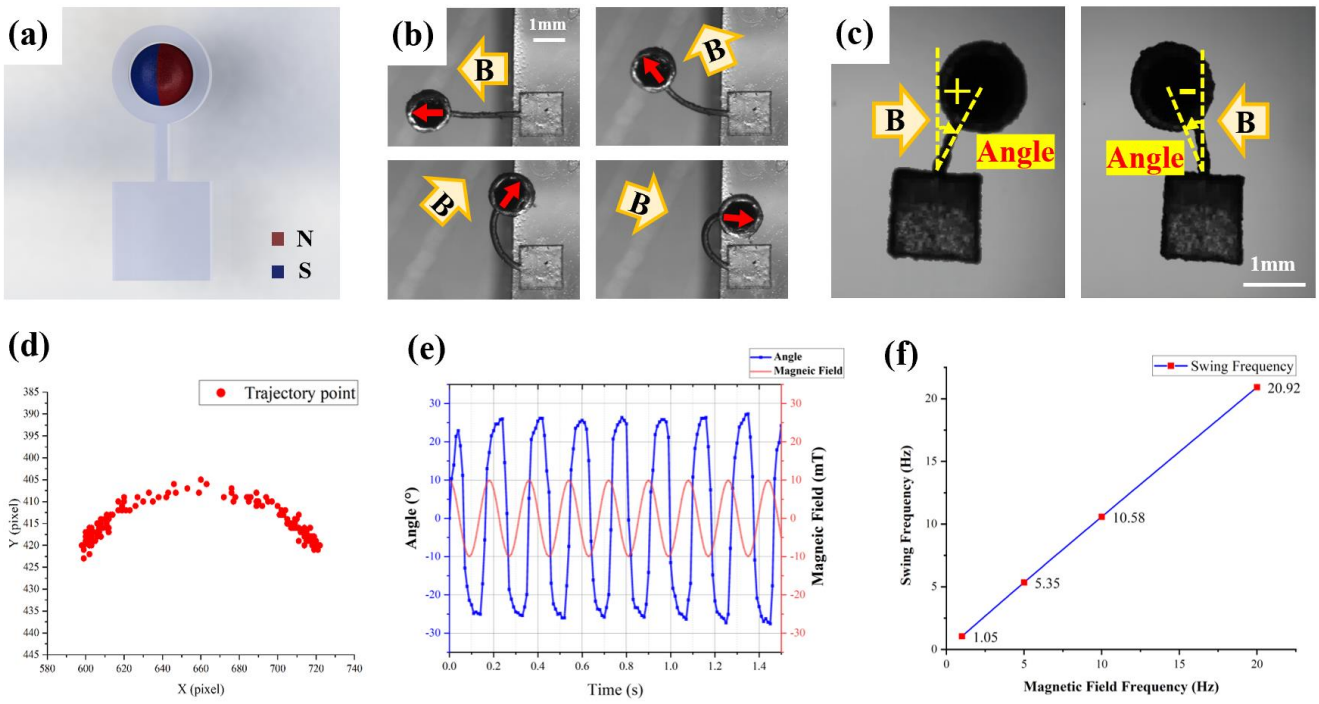

Figure 6. (a) Model diagram of magnetic microcilium robot. (b) Deformation amplitude of microcilium robot under magnetic field in different directions. (c) The sway angle of the microcilium robot. (d) The trajectory of the microbead center under a 5Hz alternating magnetic field. (e) The variation of sway angle over time. (f) The sway frequencies under different magnetic field frequencies.

passed through several filter screens with different sizes of filter hole diameter. The beads of different sizes were collected from the filter screens and placed in the glass container using absolute ethyl alcohol to rinse. The absolute ethyl alcohol could reduce the adhesion between PDMS microbeads or between the beads and the glass. Step 5: Magnetization. The fabricated magnetic beads were collected and placed separately on a glass slide. The magnetization process was executed under the externally applied magnetic field with a magnitude of 1.5mT, which lasted 5 minutes.

The production process of the soft frame is shown in Figure 5(b). First, silicone A and B were mixed evenly and then degassed to avoid bubbles. Then the mixture was applied onto the glass sheet, which was then placed on the spin-coater table. After a period of spin-coating, the mixture was evenly spread on the glass sheet and then heated on a hot plate at 70 ° C for half an hour to cure. Finally, a UV laser cutter was employed to cut silicone into the frame according to the desired pattern.

B. Experimental Results

Different types of microrobots can be fabricated by the automated assembly method proposed in this paper. As shown in Figure 6(a), a magnetic microcilium robot was fabricated to test the response speed and deformation amplitude of the microbead-frame structure under the magnetic field. In Figure 6(b), the microcilium robot could quickly and accurately sway in the same direction as the magnetic field, whose microbead magnetic direction had turned 90° left compared to Figure 6(a). The sway angle of the microcilium robot was defined as the angle between two yellow dashed lines in Figure 6(c). Figure 6(d) shows the trajectory of the microbead center during multiple consecutive swaying processes, verifying its good motion stability. Figure 6(e) shows the variation of sway angle over time under an uniaxial sinusoidal magnetic field of 5Hz. From the relationship between the sway angle and magnetic field, it can be seen that the microcilium robot can stably follow the magnetic field to sway, although there was a tiny delay degree. Figure 6(f) shows the relationship between the sway frequency and the magnetic field frequency. As the magnetic field frequency increased, the robot could still sway steadily at the same frequency as the magnetic field.

The model diagram of the hexapod magnetic soft robot mentioned earlier is shown in Figure 7(a). Figure 7(b) shows that each leg could swing as our expectations under a horizontal magnetic field, proving the reliability of automated assembly. By applying an alternating magnetic field, the robot could swim forward through the staggered swinging of each leg. In order to overcome buoyancy and achieve underwater swimming, a laser-cut carbon fiber strip was bonded to the backbone of the frame, as shown in Figure 7(c). Figure 7(d) shows the displacement of underwater swimming in the X and Y directions over time under a 5Hz sinusoidal magnetic field, which exhibited motion stability with an average swimming speed of 0.816mm/s.

At present, the assembly system can only fabricate planar microrobots with simple structures at the millimeter level, with magnetic microbead diameters around a few hundred micrometers. In fact, the manipulation precision of our microhand can reach a few micrometers [23], [24]. The main challenge lies in the micro-fabrication technology, making it difficult to produce smaller soft frames and magnetic microbeads, preventing the assembly of smaller microrobots. Furthermore, the orientation error in the direction of the microbeads is still around 20°, attributed to the resistance of UV-curing adhesives to the rotation of the microbeads.

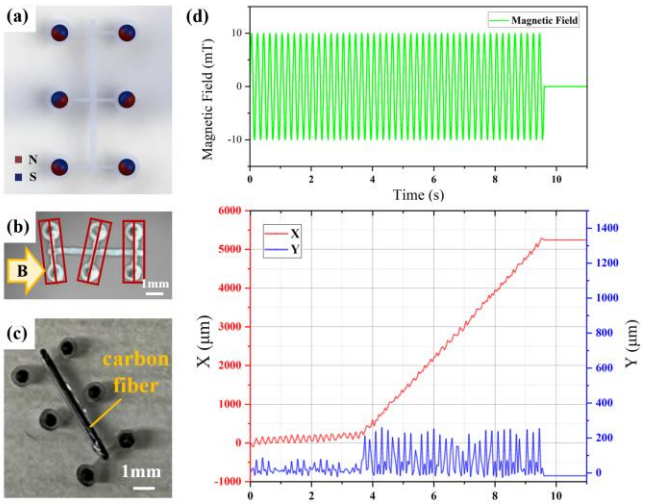

Figure 7. (a) Model diagram of swimming hexapod magnetic soft robot. (b) The swing of robot legs under a magnetic field. (c) Hexapod microrobot with added carbon fiber strip. (d) The displacement in the X and Y directions of underwater swimming.

V. Conclusion

This paper proposes a method for fabricating soft magnetic microrobots by automated assembly using a two-fingered microhand. It has been proved that this method can fabricate various magnetic robots with excellent deformation ability and locomotion performance. Compared to traditional manual assembly and assembly combined with 3D printing, this method combines manipulation flexibility with high precision and efficiency by automated assembly. In the future, further efforts can focus on constructing complex 3D structures, designing more modules with different shapes and materials, and exploring assembly methods on a smaller scale. We believe that more intelligent magnetic soft microrobots can be fabricated by this method for applications in robotics, biological measurement, and environmental detection.

References

[1] Z. Ren, W. Hu, X. Dong, and M. Sitti, "Multi-functional soft-bodied jellyfish-like swimming," *Nat. Commun.*, vol. 10, no. 1, pp. 2703, 2019.

[2] A. Nojoomi, H. Arslan, K. Lee, and K. Yum, "Bioinspired 3D structures with programmable morphologies and motions," *Nat. Commun.*, vol. 9, no. 1, pp. 3705, 2018.

[3] W. Hu, G. Z. Lum, M. Mastrangeli, and M. Sitti, "Small-scale soft-bodied robot with multimodal locomotion," *Nature*, vol. 554, no. 7690, pp. 81-85, 2018.

[4] J. Choi, J. Hwang, J. Kim, and H. Choi, "Recent progress in magnetically actuated microrobots for targeted delivery of therapeutic agents," *Adv. Healthc. Mater.*, vol. 10, no. 6, pp. 2001596, 2021.

[5] H. Ceylan, I. C. Yasa, U. Kilic, W. Hu, and M. Sitti, "Translational prospects of untethered medical microrobots," *Prog. Biomed. Eng.*, vol. 1, no. 1, pp. 012002, 2019.

[6] M. Safdar, S. U. Khan, and J. Jänis, "Progress toward catalytic micro-and nanomotors for biomedical and environmental applications." *Adv. Mater.*, vol. 30, no. 24, pp. 1703660, 2018.

[7] M. Sitti, "Miniature soft robots—road to the clinic," *Nat. Rev. Mater.*, vol. 3, no. 6, pp. 74-75, 2018.

[8] X. Z. Chen *et al.*, "Hybrid magnetoelectric nanowires for nanorobotic applications: fabrication, magnetoelectric coupling, and magnetically assisted in vitro targeted drug delivery," *Adv. Mater.*, vol. 29, no. 8, pp. 1605458, 2017.

[9] D. Fan *et al.*, "Subcellular-resolution delivery of a cytokine through precisely manipulated nanowires," *Nat. Nanotechnol.*, vol. 5, no. 7, pp. 545-551, 2010.

[10] G. Loget, A. Kuhn, "Electric field-induced chemical locomotion of conducting objects," *Nat. Commun.*, vol. 2, no. 1, pp. 535, 2011.

[11] X. Lin, Z. Wu, Y. Wu, M. Xuan, and Q. He. "Self-propelled micro-/nanomotors based on controlled assembled architectures," *Adv. Mater.*, vol. 28, no. 6, pp. 1060-1072, 2016.

[12] V. Garcia-Gradilla *et al.*, "Functionalized ultrasound-propelled magnetically guided nanomotors: Toward practical biomedical applications," *ACS Nano*, vol. 7, no. 10, pp. 9232-9240, 2013.

[13] H. Xie *et al.*, "Reconfigurable magnetic microrobot swarm: Multimode transformation, locomotion, and manipulation," *Sci. Robot.*, vol. 4, no. 28, pp. eaav8006, 2019.

[14] Y. Mirzae, O. Dubrovski, O. Kenneth, K. I. Morozov, and A. M. Leshansky, "Geometric constraints and optimization in externally driven propulsion," *Sci. Robot.*, vol. 3, no. 17, pp. eaas8713, 2018.

[15] M. Xie *et al.*, "Bioinspired soft microrobots with precise magneto-collective control for microvascular thrombolysis," *Adv. Mater.*, vol. 32, no. 26, pp. 2000366, 2020.

[16] J. Zhang, Y. Guo, W. Hu, and M. Sitti, "Wirelessly actuated thermo-and magneto-responsive soft bimorph materials with programmable shape-morphing," *Adv. Mater.*, vol. 33, no. 30, pp. 2100336, 2021.

[17] Y. Dong *et al.*, "Untethered small-scale magnetic soft robot with programmable magnetization and integrated multifunctional modules," *Sci. Adv.*, vol. 8, no. 25, pp. eabn8932, 2022.

[18] J. Zhang *et al.*, "Voxelated three-dimensional miniature magnetic soft machines via multimaterial heterogeneous assembly," *Sci. Rob.*, vol. 6, no. 53, pp. eabf0112, 2021.

[19] T. Xu, J. Zhang, M. Salehizadeh, O. Onaizah, and E. Diller, "Millimeter-scale flexible robots with programmable three-dimensional magnetization and motions," *Sci. Rob.*, vol. 4, no. 29, pp. eaav4494, 2019.

[20] Z. Li, Y. P. Lai, and E. Diller, "3D Printing of Multilayer Magnetic Miniature Soft Robots with Programmable Magnetization," *Adv. Intell. Syst.*, pp. 2300052, 2023.

[21] Z. Liu, M. Li, X. Dong, Z. Ren, W. Hu, and M. Sitti, "Creating three-dimensional magnetic functional microdevices via molding-integrated direct laser writing," *Nat. Commun.*, vol. 13, no. 1, pp. 2016, 2022.

[22] X. Hu *et al.*, "Magnetic soft micromachines made of linked microactuator networks," *Sci. Adv.*, vol. 7, no. 23, pp. eabe8436, 2021.

[23] A.A. Ramadan, T. Takubo, Y. Mae, K. Oohara, and T. Arai, "Developmental process of a chopstick-like hybrid-structure two-fingered micromanipulator hand for 3-D manipulation of microscopic objects," *IEEE Trans. Ind. Electron.*, vol. 56, no. 4, pp.1121-1135, 2009.

[24] E. Avci, K. Ohara, C.N. Nguyen, C. Theeravithayangkura, M. Kojima, T. Tanikawa, Y. Mae, and T. Arai, "High-speed automated manipulation of microobjects using a two-fingered microhand," *IEEE Trans. Ind. Electron.*, vol. 62, no. 2, pp.1070-1079, 2014.